Engineering Geology 304 (2022) 106697

Contents lists available at ScienceDirect

Engineering Geology

journal homepage: www.elsevier.com/locate/enggeo

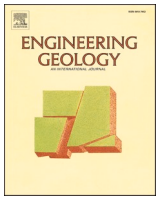

Permeable rock matrix sealed with microbially-induced calcium carbonate precipitation: Evolutions of mechanical behaviors and associated microstructure

Chenpeng Song [a,b,c], Derek Elsworth [b], Yunzhong Jia [d,*], Junzhi Lin [a]

[a] Key Laboratory of Hydraulic and Waterway Engineering of the Ministry of Education, Chongqing Jiaotong University, Chongqing, China
[b] Department of Energy and Mineral Engineering and of Geosciences, EMS Energy Institute and G3 Center, Pennsylvania State University, University Park, PA 16802, USA
[c] State Key Laboratory Cultivation Base for Gas Geology and Gas Control, Henan Polytechnic University, Jiaozuo 454000, China
[d] Department of Earth Sciences, Uppsala University, Uppsala 75236, Sweden

ARTICLE INFO

Keywords:
Microbially-induced calcium carbonate precipitation (MICP)
Bio-grouting
Permeable rock matrix
Mechanical behavior
Strength
Modulus

ABSTRACT

Microbially-induced calcium carbonate precipitation (MICP) is a promising grouting material for subsurface remediation due to its water-like viscosity and excellent penetration. Current studies of MICP-grouting for subsurface remediation of both rock fractures and highly-permeable rock matrix focus on the spatio-temporal distribution of precipitated bio-$CaCO_3$ and the resulting reduction in permeability. Conversely, we focus on the improvement of mechanical response following MICP-grouting. We contrast the improved mechanical response of MICP-treated Berea sandstones with distinctly contrasting initial mechanical properties - contrasting associated pre- and post-treatment microstructures with various durations of MICP-grouting. Results indicate that although the precipitated $CaCO_3$ mass with time within these two rock types is similar, significant differences exist in the evolution of mechanical properties (UCS, Young's modulus and brittleness). The evolution of mechanical properties for the low-strength sandstone (initial UCS 25.7 MPa) exhibits three contrasting phases: an initial slow increase, followed by a rapid-increase and then saturation and asympotic response. After ten cycles of MICP-grouting, UCS, elastic modulus and brittleness index for low-strength sandstone increase by 229%, 179% and 177% compared with before grouting. In contrast, the mechanical properties for the high-strength sandstone (initial UCS 65.1 MPa) are not significantly enhanced, increasing UCS by only 22%, 14% and 12%. Imaging by scanning electron microscopy (SEM) indicates that the cementing minerals fill the quartz framework for the high-strength sandstone but are sparse for the low-strength sandstone. Sandstone is a clastic sedimentary rock consisting of a framework of quartz grains bonded by cementing minerals. For the high-strength sandstone infused with a large mass of cementing minerals, the calcium carbonate crystals only precipitate in the gaps between the cementing minerals or adhere to the cementing minerals. This is only capable of relatively limited enhancement in the bio-bonding strength and volume of the quartz framework. For the low-strength sandstone with fewer cementing minerals, the precipitated calcium carbonate is evenly distributed on the surfaces of the quartz gains. The bulk strength is progressively increased with the ongoing bio-cementation between quartz gains. Cementing mineral contents not only exert a considerable control on the integral mechanical properties and penetration for the sandstone, but also have a direct influence on the microscopic distribution of bio-accumulated $CaCO_3$, controlling the effectiveness of bio-cementation by incrementing the mechanical properties.

1. Introduction

Microbially-induced calcium carbonate ($CaCO_3$) precipitation (MICP) is typically facilitated by the *Sporosarcina pasteurii* (*S. pasteurii*) bacterium. This bacterium mediates a series of biochemical reactions that induce the precipitation of calcium carbonate from calcium ions within a urea source (Bhaduri et al., 2016; Cardoso et al., 2020; Fan et al., 2009; Liu et al., 2017). *S. pasteurii* can catalyze the hydrolysis of urea into ammonium (NH^{4+}) and carbonate (CO_3^{2-}) by secreting urease enzyme in its metabolism. When this hydrolysis reaction occurs in the

* Corresponding author at: Department of Earth Sciences, Villavägen 16, SE-752 36 Uppsala, Sweden.
E-mail address: yunzhong.jia@geo.uu.se (Y. Jia).

https://doi.org/10.1016/j.enggeo.2022.106697
Received 23 January 2022; Received in revised form 27 April 2022; Accepted 3 May 2022
Available online 7 May 2022

presence of dissolved calcium ions, the carbonate generated from the urea hydrolysis will first precipitate as amorphous calcium carbonate and then crystallize to vaterite or calcite - with the microorganisms acting as the nucleation sites for crystal growth (DeJong et al., 2010; Liu et al., 2020; Rebata-Landa, 2007; Van Paassen, 2009). The hydroxide (OH^-) generated from the hydrolysis of the urea results in a pH increase, providing favorable conditions for calcium carbonate precipitation. Ureolysis-driven calcium carbonate precipitation by *S. pasteurii* has attracted considerable attention as a bio-cement that can both strengthen and reduce the permeability of geomaterials (Cheng et al., 2021; Liu et al., 2021; Salifu et al., 2016). Compared with cement-based or chemical grouts, MICP-grouting fluids have water-like viscosity (about 1.5 times that of water) and a very fine entrained particle size (0.5–5 μm for individual bacterial cells, average 2.8 μm (Minto et al., 2017)), thus resulting in excellent penetrability. Thus, these fluids are optimal for sealing small aperture fractures and pores with only low injection pressures (Tobler et al., 2018). In addition, bio-$CaCO_3$ is highly durable enabling sealing for >10,000 years compared with chemical grouts with limited lifespans of only ~10–20 years (Matsubara, 2021; Minto et al., 2017; Shaffer, 2010; Wu et al., 2019). Therefore, MICP is considered a promising alternative to cement and chemical grouts, especially for subsurface remediation. This includes in controlling the diffusion of contaminated groundwater, isolating deep geological disposal of nuclear waste, strengthening wellbore cements, enhancing oil recovery and in strengthening mylonitized-soft coal (Anbu et al., 2016; Cunningham et al., 2014; Kirkland et al., 2019; Phillips et al., 2018; Phillips et al., 2013; Song et al., 2021; Song and Elsworth, 2018; Song and Liu, 2020; Wu et al., 2017).

Current evaluations of MICP-grouting in rock focus on the evolution of permeability and associated microtextures of the MICP-treated fractured rock and permeable rock matrix, as well as the factors affecting the efficiency and distribution of ureolytic bacteria-driven calcium carbonate precipitation (Minto et al., 2017; Minto et al., 2016; Mortensen et al., 2011; El Mountassir et al., 2014; Song et al., 2019; Tobler et al., 2018; Tobler et al., 2014; Tobler et al., 2012; Wu et al., 2019). Few studies assess the impacts on mechanical properties of fractures and matrix after MICP-grouting. Peak fracture shear strength is shown to correlate with the percentage of the calcium carbonate cemented fracture area (Tobler et al., 2018). Prior studies have also explored the evolution of mechanical properties in Berea sandstone with the increase of calcium carbonate precipitation (Yasuhara et al., 2017). This study adopted urease enzyme instead of ureolytic bacteria to catalyze the urea hydrolysis into ammonium and carbonate, resulting in calcium carbonate precipitation. Although the chemical mechanism of enzyme-induced carbonate precipitation (EICP) is essentially the same as that for ureolytic MICP, the calcium carbonate induced by these two pathways has significant differences in crystal morphology and size (Meng et al., 2021a). More importantly, enzymatically induced calcium carbonate lacks stickiness. Conversely, in the MICP process, ureolytic microorganisms secrete urease enzyme to catalyze urea hydrolysis and also secrete extracellular polymeric substances (EPS) into their environment as high-molecular-weight polymer film (nanoscale thickness) that is cohesive (Sheng et al., 2010; Song and Elsworth, 2020). EPS not only imparts cohesion to the biomineralized calcium carbonate, but also plays a controlling role in capturing calcium ions, the precipitation and crystal growth of calcium carbonate (Tourney and Ngwenya, 2009). Therefore, the calcium carbonate induced by each of urease and ureolytic bacteria has essential differences in mineralization mechanism, microscopic features and physical properties.

In this study, we investigate the evolution of mechanical properties and associated microscopic structure of rock matrix penetrated by MICP-grouts. Specifically, two contrasting Berea sandstones with distinctly different initial mechanical properties are subjected to various durations of MICP-grouting. Changes in pre- and post-peak strength, elastic modulus and brittleness are measured and contrasted against the microscopic evolution of the rock matrix and the distribution of the bio-accumulated $CaCO_3$ using SEM. Mechanistic models unifying these observations between internal structure and the macro-mechanical characteristics are advanced.

2. Experimental methods

The experimental sequence is summarized in Fig. 1. The prepared sandstone cores are first characterized for initial porosity and permeability before being MICP-grouted in 2, 4, 6, 8 and 10 cycles. The post-treated cores are re-examined for porosity and permeability and the mass of calcium carbonate precipitated within each sample measured. Subsequently, uniaxial compression tests evaluate peak strength, brittleness and elastic modulus for these sandstone cores for contrasting durations of MICP-grouting cycles. Post-failure, the mineral compositions, micromorphology of the precipitated $CaCO_3$ and its distribution within sandstone matrix are examined by X-ray diffraction (XRD) and scanning electron microscopy (SEM).

2.1. Preparation of sandstone samples

Two contrasting sandstones with distinctly different strengths and moduli are obtained from the Devonian in Ohio, USA (Berea sandstone). One has a higher permeability but lower strength, and the other has a lower permeability and higher strength. The sandstone blocks are cored into 1-in. (25.4 mm) diameter cylindrical samples and then trimmed to 2-in. (50.8 mm) in length. We measure the initial porosity and permeability for these sandstone cores and select six cores of each type for which porosity and permeability are closest – and use these as the candidates for MICP-grouting. The petrophysical properties of these two types of Berea sandstone are shown in Table 1. The porosity is determined by helium porosimetry, and the permeability is measured for steady flow based on Darcy's law. Table 1 defines properties for the high permeability and low strength Berea and for the low permeability and high strength material – as referenced in the following text as low (HS) and high (LS) strength sandstones.

2.2. Bacteria cultivation

The particular strain of *S. Pasteurii* is purchased from the American Type Culture Collection (freeze-dried, ATCC 11859). The growth medium is the NH4-YE liquid medium (ATCC 1376). The strain is first

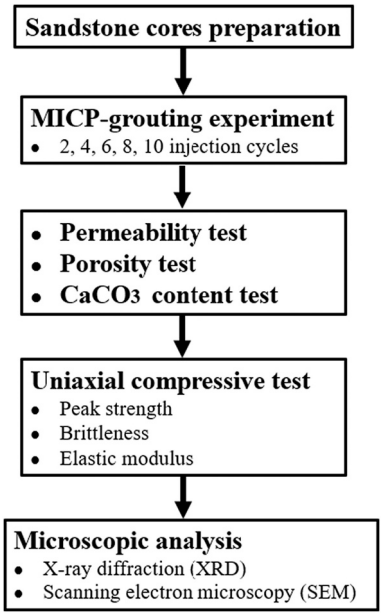

Fig. 1. Summary of the experiential sequence.

Table 1
Petrophysical properties of these two types of Berea sandstone.

Name	Porosity (−)	Permeability (mD)	UCS (MPa)*	Young's Modulus (GPa)*
Type-1 (LS)	19.17–19.45%	102.1– 106.8 (higher)	25.71 (lower)	4.57
Type-2 (HS)	17.27–17.33%	17.2– 18.7 (lower)	65.11 (higher)	7.51

* Uniaxial Compressive Strength (UCS) and Young's Modulus are determined from one of the six sandstone cores of each type.

activated and then cultured at 30 °C in a shaking water bath (200 r/min) for 24–36 *h* before harvesting at $OD_{600} = 1.0$. OD_{600} is an abbreviation referring to the optical density of a sample measured at a wavelength of 600 nm - a standard classification in estimating the concentration of bacterial or other cells in a liquid (Sutton, 2011). The bacterial culture is then centrifuged at 4000*g* for 30 mins and the supernatant fluid removed and supplemented by NH_4-YE growth medium. After repeating this centrifugation process once, the bacterial solution is stored at 4 °C prior to use.

2.3. Experimental apparatus and MICP-grouting strategy

The experimental apparatus for the MICP-grouting is illustrated in Fig. 2. The sandstone core is installed inside a fluoro rubber jacket and confined within a triaxial core holder capable of applying independent loading in the radial and axial directions. A dual cylinder syringe pump (ISCO 500D) with a control accuracy ±0.1 KPa is used to apply the radial and axial stresses with distilled water as a confining fluid. The sandstone core is constrained end-to-end between two cylindrical stainless steel loading platens with throughgoing flow connections and flow distributors (Wang et al., 2011; Zhi et al., 2019). The core and the platens are isolated from the confining fluid by the rubber jacket. The upstream platen is connected to a pump to inject MICP-fluids into the sandstone core. The experiment adopts a staged grouting strategy, that is, in a single grouting cycle, the bacterial solution is first injected into the sample, followed by the mixed solution of urea and calcium chloride. The bacterial solution and urea/$CaCl_2$ solution are injected by separate pumps and tubing to prevent calcium carbonate precipitation from occurring in the pump and influent flow lines. The downstream platen outflows at atmospheric pressure. The sandstone core is loaded to 3.0 MPa in both radial and axial directions throughout the MICP-grouting.

The sandstone cores are grouted in repeated but discrete injection cycles. A single grouting cycle contained 10 mL of *S. Pasteurii* suspension (about twice the pore volume of sample) and 25 mL of the cementation solution (1.0 mol/L $CaCl_2$ and 1.0 mol/L urea). The staged grouting strategy increases the residence time within the sample and potentially maximizes the efficiency of the grouting by producing a more homogeneous calcium carbonate distribution along the rock column (Tobler et al., 2012). In addition, before injecting the bacterial solution, 0.056 g of calcium chloride is added to 10 mL of bacterial solution (i.e. per liter of bacterial solution contained 0.05 mol $CaCl_2$). This is used to reduce the electrostatic repulsion between bacteria and sand grains, thus strengthening bacterial attachment and bacterial flocculation (Tobler et al., 2018; Tobler et al., 2012) in the subsequent calcium carbonate precipitation process. The experimental grouting schedule is shown in Fig. 3. In each subsequent grouting cycle, the MICP-fluids are reversed across the core (so that the prior injection outlet becomes the new inlet) to make the distribution of the calcium carbonate even more homogeneous within the sample. In the two successive grouting cycles, we halt injection for one hour to allow for stagnation in the sample and to prepare for the next grouting cycle. This allows the urea/$CaCl_2$ solution remaining within the pores of the sample to fully react. These two contrasting types of Berea sandstone are individually grouted by either 2, 4, 6, 8 or 10 cycles of the MICP solution – requiring 5 individual samples.

2.4. Measurements of permeability, porosity and calcium carbonate content of MICP-treated samples

After the predetermined grouting cycle is completed, the samples are left within the core holder and with no throughflow for one hour before the permeability is then measured by injection of distilled water at

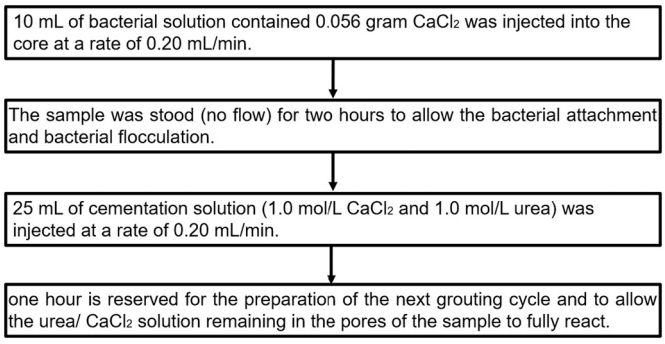

Fig. 3. Standard MICP-grouting strategy.

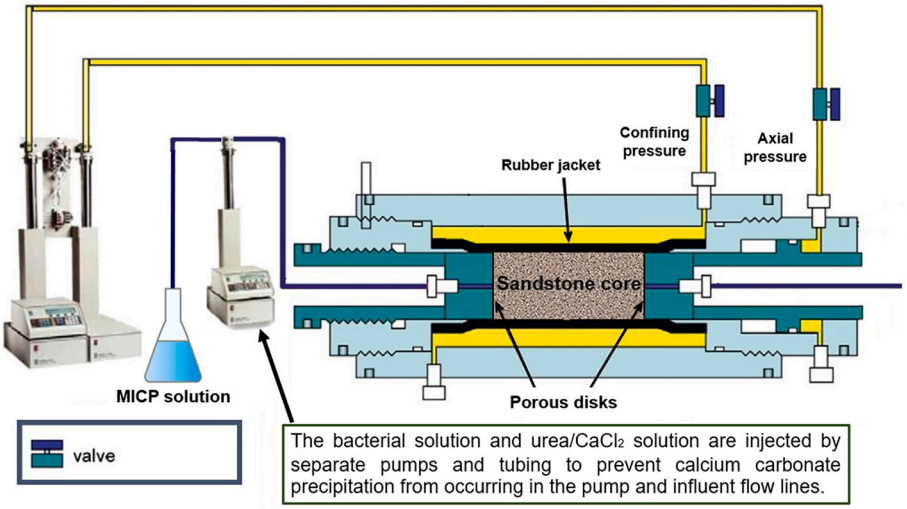

Fig. 2. Schematic of the experimental apparatus for MICP-grouting.

constant flow rate. The permeability is evaluated assuming steady flow and using Darcy's law as,

$$k = \frac{QL\mu}{\Delta pA} \quad (1)$$

where k is the permeability (m^2), Q is the flow rate (m^3/s), L is the core length (m), μ is the dynamic viscosity of the fluid (Pa·s), ΔP is the pressure difference from the inlet to the outlet (Pa), and$A$ is the cross-sectional area of the sample (m^2).

Following the permeability measurement, the sandstone core is removed from the holder, dried at 80 °C for 24 h, and the porosity and calcium carbonate content determined. The change in the porosity of the sandstone cores post-grouting is determined by helium porosimetry. The calcium carbonate ($CaCO_3$) content of the MICP-treated core is determined by measuring the oven-dry difference in mass of the cores before and after -grouting and expressed as the mass of calcium carbonate per unit volume of sandstone (g/cm^3).

2.5. Changes in strength (UCS), modulus and brittleness of grouted samples

The pre- and post-peak mechanical properties of the MICP-treated sandstone samples are measured for uniaxial compressive strength (UCS), Young's modulus and brittleness. The uniaxial compressive tests are conducted according to ASTM D7012–14 (i.e., Standard Test Methods for Compressive Strength and Elastic Moduli of Intact Rock Core Specimens under Varying States of Stress and Temperatures). The axial load was applied at a constant strain rate of 0.1 mm/min throughout the testing.

The Young's modulus is calculated from the average slope of the straight-line portion of the stress-strain curve, as per ASTM D7012–14. Brittleness relates to the ratio of strength drop (peak to residual) relative to peak strength (Meng et al., 2021b; Meng et al., 2015) to define the brittleness index (*BI*) (Holt et al., 2015). Brittleness index is defined as (Meng et al., 2015),

$$BI = \frac{\tau_p - \tau_r}{\tau_p} \frac{lg|k|}{10} \quad (2)$$

where τ_p represents uniaxial compression strength (UCS), τ_r is residual strength, and k is the slope of the line from the initial yielding point to the starting point of the residual strength. The absolute value of k is adopted as the measured slope is always negative. The value of *BI* ranges from 0 to 1 with a higher *BI* value indicating higher brittleness.

3. Experimental results

3.1. Permeability, porosity and calcium carbonate content of MICP-treated sandstone cores

Changes in permeability with the progress of MICP-grouting cycles are shown in Fig. 4(a). Overall, the permeabilities for both of the LS and HS sandstones significantly decline with increasing duration of grouting. Specifically, the permeability of the high-permeability sandstone (LS sandstone in Fig. 4(a)) core reduces by ~96% from 105.7 mD to 4.19 mD after 10 cycles of grouting, while the permeability of the low-permeability sandstone (HS sandstone in Fig. 4(a)) with 10 cycles grouting declines from 18.4 mD to 0.20 mD, reducing by ~99%. We also compare the normalized permeability reduction between these two sandstone cores with increasing number of cycles of grouting by normaizing relative to the initial permeability (Fig. 4(b)). As shown in Fig. 4 (b), the permeability reduction (effective permeability) for the low-permeability samples indicates greater sensitivity than that for the high-permeability samples for identical durations (numbers of cycles) of MICP-grouting. This is consistent with a presumed greater reduction in pore throat diameter occurring for the narrower pore throats of the low-permeability sandstones.

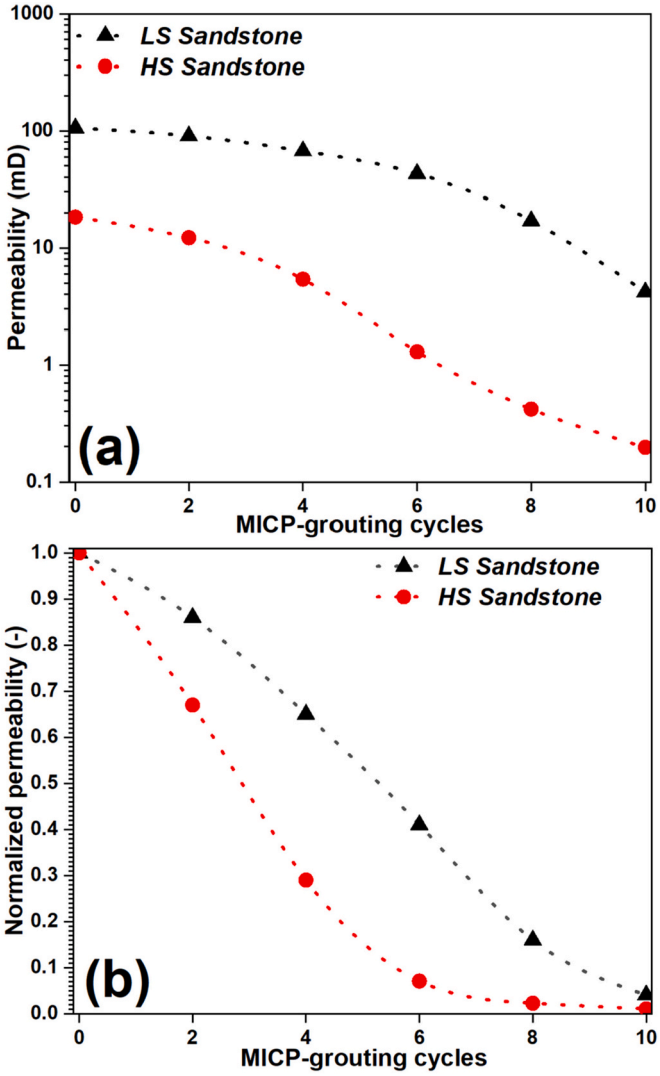

Fig. 4. Variation in permeability and normalized (effective) permeability after 0, 2, 4, 6, 8 and 10 cycles of MICP-grouting. (a) Permeability. (b) Normalized permeability.

Following the permeability measurement, the porosity of the sandstone cores, subject to various numbers of MICP-grouting cycles, is determined by helium porosimetry. As shown in Fig. 5, the porosity decreases linearly with increasing cycling of bio-treatment. After 10 cycles of MICP-treatments, the porosity of the high-permeability sample (LS sandstone) decreases from 19.19% to 10.88%, while the low-permeability sample (HS sandstone) decreases from 17.28% to 10.46%.

Subsequently, we further measure the change in oven-dry mass of the sandstone cores before and after grouting to obtain the precipitated calcium carbonate mass for different MICP-treatments (Fig. 6(a)). The calcium carbonate content within the samples is expressed as the mass of calcium carbonate per unit volume of sandstone (g/cm^3). The measured calcium carbonate content of high-permeability samples (LS sandstone) is slightly higher than that of the low-permeability samples (HS sandstone) for equivalent durations of MICP-grouting. Previous studies have indicated that the injected microfluid velocity of the cementation solution (urea-Ca^{2+}) can affect the efficiency of the MICP-reactants. When the reaction rates of the microbially-driven urea hydrolysis and calcium carbonate precipitation are faster than the input rate of urea-Ca^{2+} solution, more calcium ions can be precipitated under the same conditions (Al Qabany et al., 2012; Song and Liu, 2020). In other words, a lower

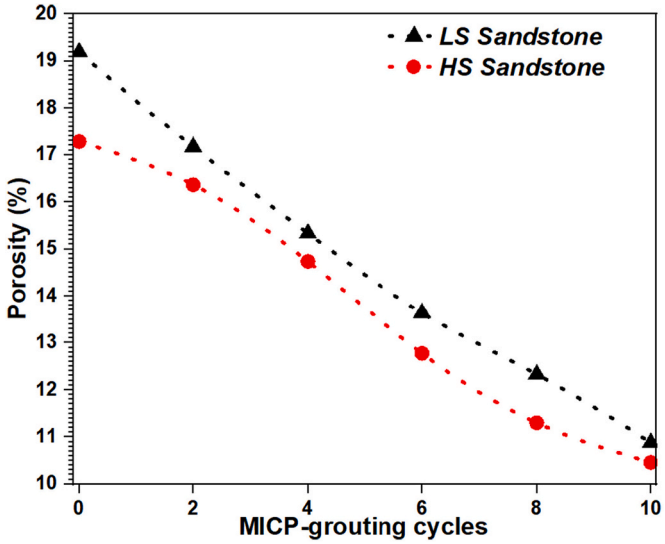

Fig. 5. Variation in porosity for the sandstone samples after 0, 2, 4, 6, 8 and 10 cycles of MICP-grouting.

fluid velocity of urea-Ca^{2+} solution through the pore can contribute to a higher $CaCO_3$ precipitation efficiency. The low-permeability sandstone presumably has narrower pore throats than the high-permeability samples, resulting in the microfluid velocity through the pore spaces within the low-permeable sample being higher than that for the high-permeability sample at the identical volumetric flow rates. Therefore, the harvestable calcium carbonate mass within the high-permeability samples is larger than that of the low-permeability samples for identical durations of MICP-treatment. In addition, we quantitatively calculated the change in the conversion rate of calcium ions in the urea-Ca^{2+} solution with increasing MICP-treatments. The Ca^{2+} conversion rate is defined as,

$$Ca^{2+}\ \text{conversion rate}\ (\%) = \frac{m_n}{M \times n} \times 100\% \quad (3)$$

where m_n represents the mass of precipitated calcium carbonate within the sandstone core after n cycles of MICP-grouting, M represents the maximum theoretical mass of calcium carbonate precipitation that can be synthesized in a single MICP-grouting. That is, 100% of the calcium ions within the urea-Ca^{2+} solution of a single grouting cycle is precipitated into calcium carbonate (each cycle of MICP-grouting can produce up to 2.5 g of calcium carbonate). Fig. 6(b) shows the average Ca^{2+} conversion rate after 2, 4, 6, 8 and 10 cycles of MICP-grouting, respectively. Clearly, with increasing MICP-cycles, the efficiency of precipitation of the microbially-mediated calcium carbonate gradually decreases – potentially as the consequence of the increase in microfluid velocity. As the precipitated $CaCO_3$ continuously accumulates, the pore spaces become progressively narrower, resulting in an increase in the flow velocity of the urea-Ca^{2+} solution through the pore throats and a reduction in the efficiency of microbially-induced calcium carbonate precipitation.

3.2. Evolution of mechanical properties

We determine trends in peak strength, Young's modulus and brittleness of these sandstones with increase in the number of MICP-grouting cycles by measuring pre- and post-peak strengths of the samples. The stress-strain curves for these two sandstone cores following various durations/cycles of MICP-grouting are shown in Fig. 7 - with corresponding peak strengths also marked. Overall, the low-strength samples (LS-HP sandstone, Fig. 7 (a)) indicate a proportionately higher gain in peak strength with an increase in grouting cycles. After

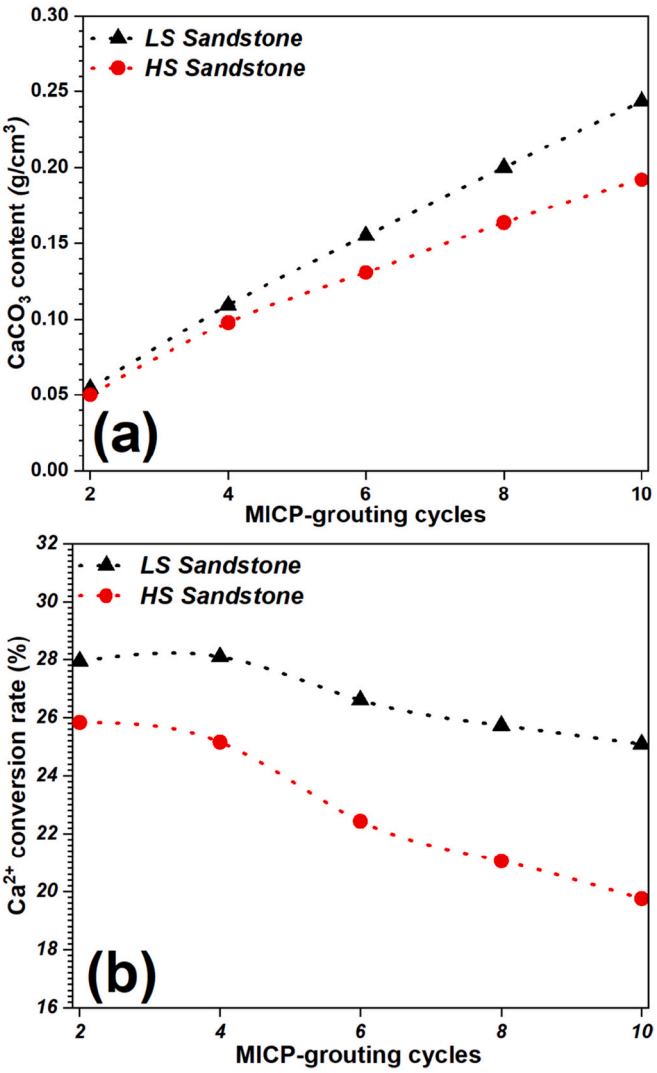

Fig. 6. Variation in $CaCO_3$ content and the average Ca^{2+} conversion rate of MICP within these two sandstones after 0, 2, 4, 6, 8 and 10 cycles of MICP-grouting. (a) $CaCO_3$ content. (b) Average Ca^{2+} (urea-Ca^{2+} cementation solution) conversion rate.

10 cycles, the uniaxial compressive strength (UCS) for the low-strength sandstone sample increased from 25.71 MPa to 58.96 MPa, ~2.3 times that of the untreated sample. Conversely, the UCS for the high-strength sample (HS-LP sandstone Fig. 7 (b)) only increases by ~22% from 65.11 MPa to 79.36 MPa. Subsequently, we calculate Young's modulus and brittleness for these biotreated samples from these same stress-strain data. We then define the correspondence between $CaCO_3$ content and UCS, Young's modulus, and brittleness. As shown in Fig. 8(a)-(c), the evolution of mechanical properties for the high-strength and low-strength sandstone samples significantly differs with increasing calcium carbonate content. The mechanical properties for the low-strength sandstone are impacted most. After ten cycles of MICP-grouting in the low-strength sandstone, UCS, Young's modulus and brittleness index increase by 229%, 179% and 177% relative to pre-grouting, Trends in evolution with the accumulation of calcium carbonate presents in three contrasting stages. For the initial $CaCO_3$ accumulation, there is only a negligible increase in strength, stiffness or brittleness. As the calcium carbonate mass continues to accumulate, the mechanical properties increase rapidly before finally reaching a plateau at large concentration. By contrast, the evolution of the mechanical properties of the high-strength sandstone increase constantly, and at low rate, throughout.

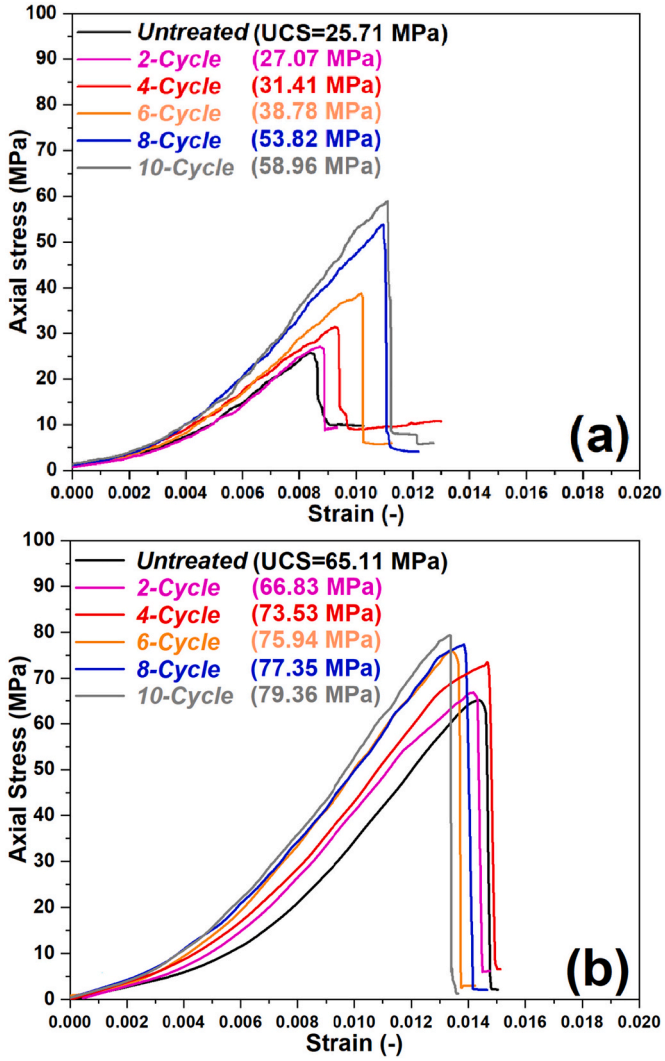

Fig. 7. Stress-strain curves for these two sandstone samples with increased MICP-grouting. (a) Low strength sandstone. (b) High strength sandstone.

After ten cycles of MICP-grouting, the UCS, Youngs's modulus and brittleness index only increase by 22%, 14% and 12% relative to pre-grouting. This observed and distinctly different evolutionary trend of mechanical behavior for these two sandstones is likely associated with the calcium carbonate distribution and related cementation within the intergranular spaces of the sandstone. We conduct microscopic characterizations of the biotreated samples to further explore this posit.

4. Microscopic phenomena and discussion

We determine the mineralogy of the precipitated calcium carbonates by X-ray diffraction (XRD) on the powdered sandstone both before and after MICP-grouting. The microscopic morphology of the microbially-induced calcium carbonate, as well as its distribution within the intergranular spaces, are examined by scanning electron microscopy (SEM) to define microscopic processes mediating bio-cementation.

4.1. Crystalline forms of microbially-induced calcium carbonate

The untreated and 10-cycle-treated MICP-grouted samples are examined by XRD. As shown in Table 2, the XRD results suggested that the raw Berea sandstone is mainly composed of quartz and small amounts of microcline, muscovite and kaolinite, while the calcite and vaterite contents increase significantly in the MICP-treated sample.

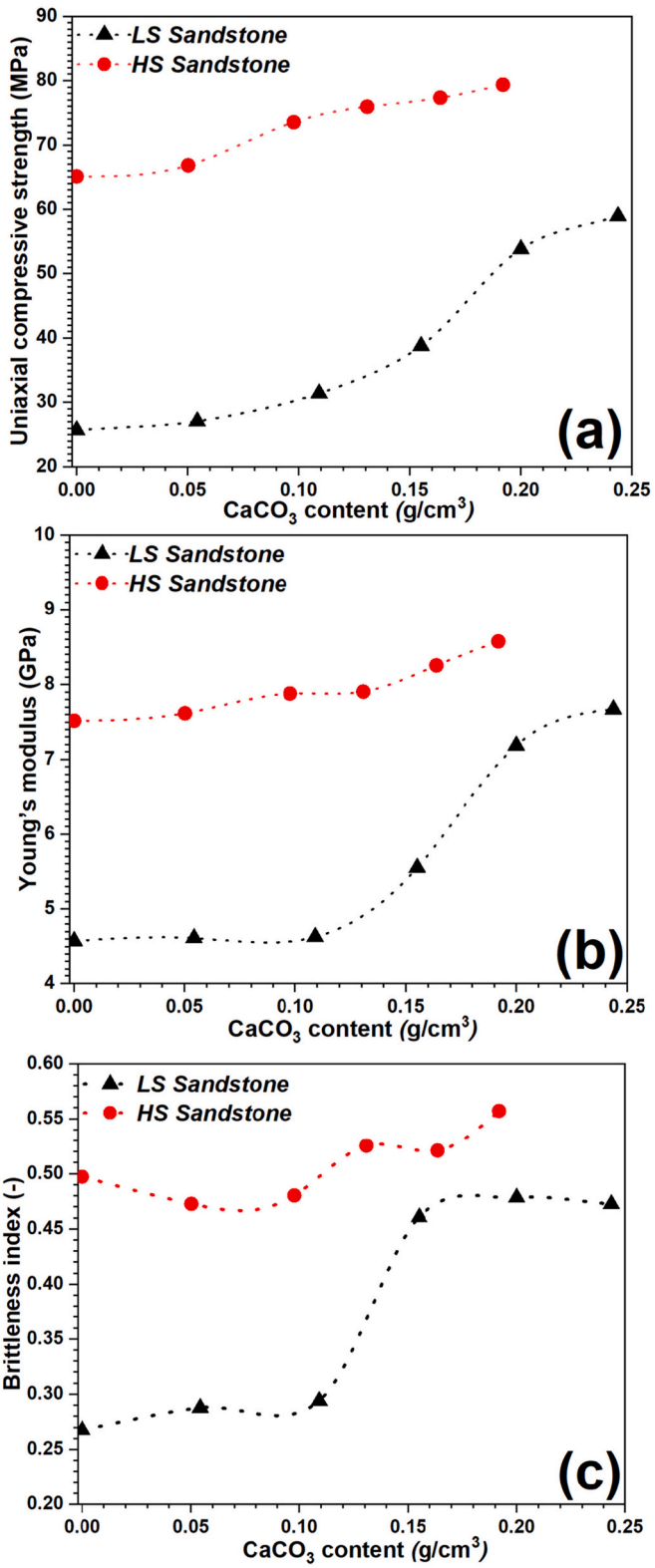

Fig. 8. Correspondence between $CaCO_3$ content and (a) UCS, (b) Young's modulus, and (c) brittleness index.

Vaterite and calcite, representing two polymorphs of calcium carbonate, are the microbially-produced components. The XRD results also imply that more than 60% of the generated calcium carbonate is calcite.

Table 2
Mineral composition of Berea Sandstone both before then after 10 cycles of MICP-grouting, as recovered from XRD.

Minerals	HP-LS Berea Sandstone		LP-HS Berea Sandstone	
	Untreated (wt %)	MICP-treated (wt%)	Untreated (wt %)	MICP-treated (wt%)
Quartz	91.6	79.5	89.6	82.4
Microcline	5.5	5.2	6.5	5.8
Muscovite	2.3	1.9	0	0
Kaolinite	0.4	0.2	3.9	2.2
Calcite	0.2	8.3	0	6.0
Vaterite	0	4.8	0	3.6

4.2. Cumulative process of microbially-induced calcium carbonate

We scan then compare the micro textures of fracture surfaces resulting from the compressive failure of the samples to define bio-$CaCO_3$ accumulation and induced intergranular bonds for these two Berea sandstones. Fig. 9(a)–(c) are SEM images of the original LS sandstones, and after four- then ten-cycles of bio-grouting, respectively. Clearly, only few cementing minerals infill the quartz framework in the untreated LS sandstones (Fig. 9(a)) – reflected in its so low bulk strength (UCS for LS sandstone is only 25.7 MPa). Sandstone is a clastic sedimentary rock consisting of a framework of quartz grains bonded by cementing minerals. Cementing minerals contents exert a considerable control on the bulk strength. With the gradual precipitation of microbially-mediated calcium carbonate, the early precipitates of $CaCO_3$ are dispersed on the surfaces of the quartz grains and occupy the rims of the pore spaces (Fig. 9(b)). As the microbially-mediated mineralization continuously accumulates, the surface coatings thicken and then fill. Consequently, the adjacent quartz grains are bonded, and the bonding strength is continuously enhanced with an increase in the bio-cementation area (Fig. 9(c)).

By contrast, the SEM images for the high-strength sandstone indicate a significant difference from the low-strength sandstone. Figs. 10(a), (b) and (c) are the SEM images for the original "LP-HS" sandstones, and after four- then ten-cycle of bio-grouting, respectively. The cementing minerals filling the quartz framework for the high-strength sandstone are clearly more than for the low-strength sandstone (Fig. 10(a)). This petrophysical observation is well aligned with the initial mechanical strengths for these two sandstones (UCS for LS sandstone is only 25.7 MPa, while HS sandstone is 65.1 MPa). Sandstone is a clastic sedimentary rock consisting of a framework of quartz grains bonded by cementing minerals. Larger masses of cementing minerals can enhance the bonding strength between quartz grains, thereby imparting a higher bulk strength. With the increased duration of MICP-grouting, most of the precipitated calcium carbonate crystals populate the gaps between the cementing minerals or adhere to cementing minerals, as shown in the SEM images of Fig. 10(b) and (c).

In addition, it is worth noting that with the accumulation of bio-$CaCO_3$, the microscopic failure of the LS sandstone under uniaxial compression changes from intergranular fracture to transgranular fracture, implying that the bio-$CaCO_3$ effectively enhances the bonding strength and bonding areas between quartz grains. In contrast, the microscopic failure of the HS sandstone is dominated by transgranular fracture. These microscopic observations are consistent with trends in the variation in mechanical properties for these two sandstones with the increasing accumulation of bio-$CaCO_3$.

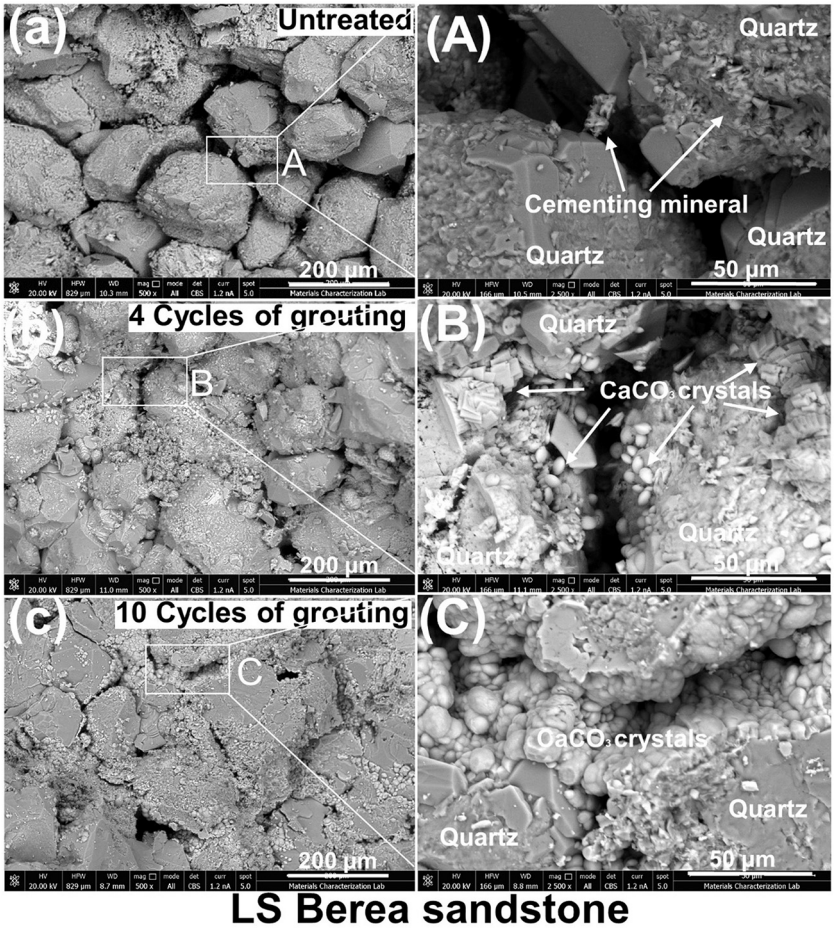

Fig. 9. Textures of bio-accumulation of $CaCO_3$ within LS sandstone.

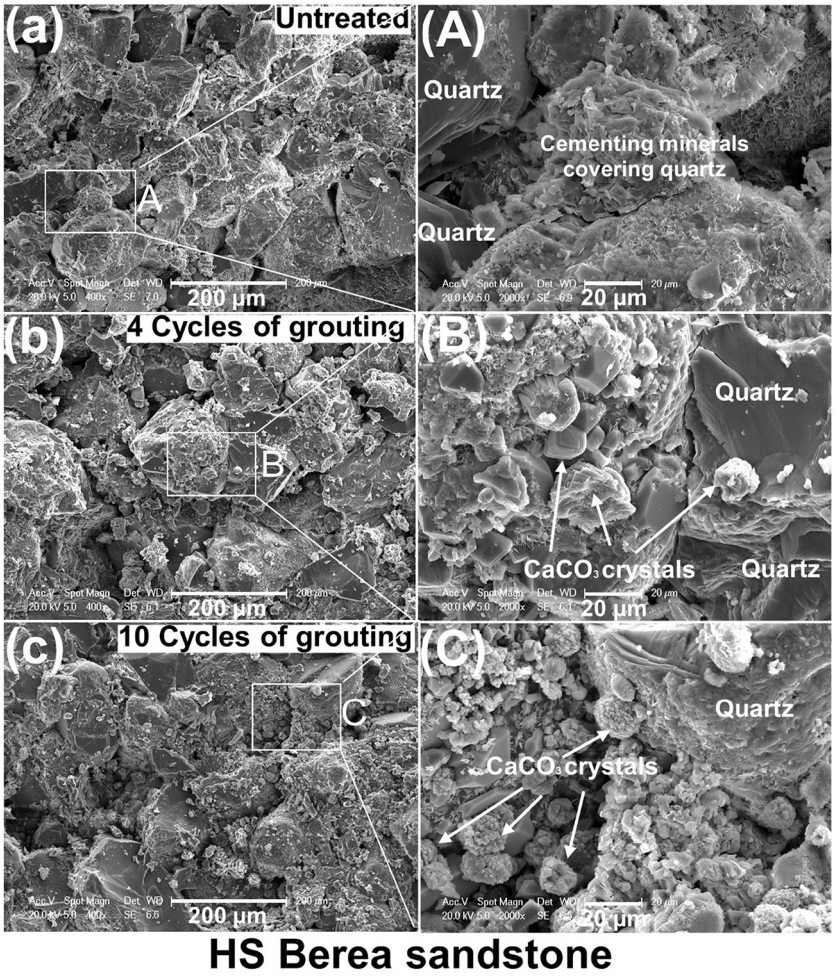

Fig. 10. Textures of bio-accumulation of $CaCO_3$ within HS sandstone.

4.3. *Evolution of mechanical behavior after MICP-grouting*

This work quantifies the evolution of mechanical properties of sandstones associated with evolving microstructures following MICP-grouting. Trends in the evolution of mechanical properties in these two sandstones that develop distinct microscale textures indicate significant differences. Sandstone is a clastic sedimentary rock consisting of a quartz framework of grains bonded by cementing minerals. The bonding exerts a considerable control on the ensemble mechanical properties and penetration of grout into the sandstone, and therefore also has a direct influence on the microscopic distribution of bio-$CaCO_3$ and its resulting cementation efficiency.

For the low-strength sandstone with fewer cementing minerals, the precipitated calcium carbonate is relatively evenly distributed on the surfaces of the quartz gains. As this mass continuously accumulates, the narrow pore spaces between quartz grains are first bonded by the precipitating calcium carbonate, with the bonding strength progressively strengthened with the ongoing bio-cementation. In addition, these narrow pores also exert a key control on the flow distribution of the MICP-grout. Once the narrow pores fill and plug, the MICP-grout will no longer flow through to the adjacent large pores, and the $CaCO_3$ accumulation in the large pores spaces also stagnates. The meager calcium carbonate precipitated in the large pores is therefore an ineffective bond to support the quartz framework-due to its limited accumulation. Based on the foregoing, in the initial stage of MICP-grouting, the intergranular bonding sites and bonding strength of bio-$CaCO_3$ are relatively limited as a result of the limited and isolated $CaCO_3$ accumulation.

Consequently, the incremental increase in the ensemble mechanical properties with fewer cementing minerals is initially comparatively gentle. This intergranular dislocation leads to macroscopic failure under uniaxial compression. As the precipitated $CaCO_3$ continuously occupies the surfaces of quartz grains, the bonding areas in the narrow voids is gradually enhanced and thus the ensemble mechanical properties increase rapidly an increase in $CaCO_3$ mass. Therefore, the microscopic failure under uniaxial compression changes from intergranular fracture to transgranular fracture. Until the narrow pore spaces are almost filled by the precipitated calcium carbonate, the growth rate in mechanical properties ultimately approaches an asymptote. This mechanistic explanation for the strength gain in the sandstone with fewer cementing minerals (low-strength sandstone) is consistent with its evolution in mechanical properties with the accumulation of $CaCO_3$. A schematic for the cumulative process of bio-$CaCO_3$ within low-strength sandstone (fewer cementing minerals) is illustrated in Fig. 11.

For the high-strength sandstone with a large mass of cementing minerals, the evolution of mechanical behaviors and its associated microstructure in response to calcium carbonate accumulation indicate clear differences with the sandstone with less cementing mass. Higher mineral contents can ensure sufficient bonding area and bonding strength between the quartz grains, thereby resulting in high bulk strength. This demonstrates the principal application of the method in its efficacy of bio-$CaCO_3$ cementation for improving mechanical properties. In addition, the narrow pore spaces within the quartz framework provide optimal sites for bio-cementation. However, for the highly cemented sandstone, these narrow pores are more likely to be narrowed-

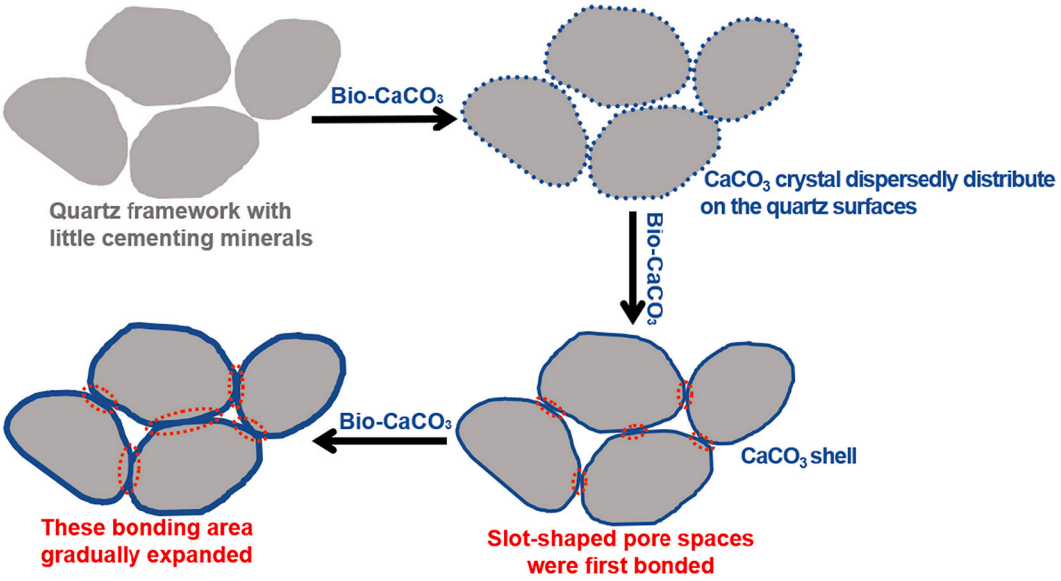

Fig. 11. Schematic describing strength gain in bio-cementation by $CaCO_3$ within sandstone with lower concentration of cementing minerals.

down and occupied by the cementing minerals during natural diagenesis. This causes the available nucleation sites and growth spaces for bio-accumulated $CaCO_3$ in the narrow pore spaces to be significantly restricted. As we have observed, the precipitated calcium carbonate crystals precipitate within the gaps between the cementing minerals or adhere to cementing minerals, which is relatively limited in enhancing the bonding strength and area within the quartz framework. These dual mechanisms likely explain why the mechanical behaviors of high-strength sandstones rich with cementing minerals do not show a significant increment with the $CaCO_3$ accumulation.

This study reveals the evolution of mechanical properties of sandstones associated with evolving microstructures following MICP-grouting – increases in UCS and deformation modulus. More importantly, it provides a basis to understand the linked characteristics of permeability reduction after MICP-grouting under changing in-situ stress conditions, which is of great significance for MICP-grouting to reduce leakage from carbon sequestration reservoirs and to enhance sweep efficiency of oil reservoirs. Current studies of MICP-grouting for permeability reduction in rock fractures and highly-permeable rock matrix rarely consider the coupling with the stress field. This is undoubtedly the focus of our next work.

5. Conclusions

This work investigates the mechanical behaviors and associated microstructure of low-strength and high-strength Berea sandstone subject to various durations of MICP-grouting. Observations indicate that although the generated $CaCO_3$ mass within these two media is relatively similar for identical durations of MICP-grouting, significant differences exist the increases in both strength and deformability (UCS magnitudes, Young's Modulus and brittleness). The variations in mechanical properties for low-strength sandstone (initial UCS = 25.7 MPa) with bio-accumulation of $CaCO_3$ undergo three contrasting phases: an initial slow increase, followed by a rapid-increase and then saturation and asymptotic response. After ten cycles of MICP-grouting, UCS, Young's modulus and brittleness index for low-strength sandstone increased by 229%, 179% and 177% compared with before grouting. By contrast, the evolution of mechanical properties for high-strength sandstone do not show a significant increment with $CaCO_3$ accumulation. In contrast, after ten cycles of MICP-grouting, UCS, elastic modulus and brittleness index for high-strength sandstone only increased by 22%, 14% and 12% compared with before grouting.

Imaging by scanning electron microscopy (SEM) indicates that for the low-strength sandstone with fewer cementing minerals, the generated calcium carbonate precipitation accumulates evenly on the surfaces of the quartz gains. As this mass continuously accumulates, the narrow pore spaces between quartz grains are first bonded by the precipitated calcium carbonate, with the bonding strength progressively strengthened with the increase in area of bio-cementation. Until these narrow pore spaces are almost filled, the growth rate in mechanical properties approaches an asymptote. For the high-strength sandstone with a large mass of cementing minerals, the efficacy of bio-$CaCO_3$ cementation for mechanical properties is likely concealed by the presence of cementing minerals. The calcium carbonate crystals only precipitate in the gaps between the cementing minerals or adhere to the cementing minerals. This is only capable of relatively limited enhancement in the bonding strength and area of the quartz framework. Cementing minerals within quartz framework not only exert a considerable control on the integral mechanical properties and penetration for the sandstone, but also have a direct influence on the microscopic distribution of bio-accumulated $CaCO_3$, controlling both the cementation efficiency and the increment of mechanical properties.

CRediT authorship contribution statement

Chenpeng Song: Conceptualization, Formal analysis, Investigation, Writing – original draft. **Derek Elsworth:** Conceptualization, Writing – review & editing. **Yunzhong Jia:** Formal analysis, Writing – review & editing. **Junzhi Lin:** Writing – review & editing.

Declaration of Competing Interest

The authors declare that they have no known competing financial interests or personal relationships that could have appeared to influence the work reported in this paper.

Acknowledgments

This work has been supported by the National Natural Science Foundation of China (Project No. 51604051), the Key Laboratory of Hydraulic and Waterway Engineering of the Ministry of Education (Project No. SLK2021B04), and the State Key Laboratory Cultivation Base for Gas Geology and Gas Control (Project No. WS2020A02). The authors are grateful for this support.

References

Al Qabany, A., Soga, K., Santamarina, C., 2012. Factors affecting efficiency of microbially induced calcite precipitation. J. Geotech. Geoenvironmental Eng. 138, 992–1001. https://doi.org/10.1061/(ASCE)GT.1943-5606.0000666.

Anbu, P., Kang, C.H., Shin, Y.J., So, J.S., 2016. Formations of calcium carbonate minerals by bacteria and its multiple applications. Springerplus. 5 (1), 1–26. https://doi.org/10.1186/s40064-016-1869-2.

Bhaduri, S., Debnath, N., Mitra, S., Liu, Y., Kumar, A., 2016. Microbiologically Induced Calcite Precipitation Mediated by Sporosarcina pasteurii. J. Vis. Exp. 110, e53253 https://doi.org/10.3791/53253.

Cardoso, R., Pedreira, R., Duarte, S.O., Monteiro, G.A., 2020. About calcium carbonate precipitation on sand biocementation. Eng. Geol. 271, 105612 https://doi.org/10.1016/j.enggeo.2020.105612.

Cheng, Y.J., Tang, C.S., Pan, X.H., Liu, B., Xie, Y.H., Cheng, Q., Shi, B., 2021. Application of microbial induced carbonate precipitation for loess surface erosion control. Eng. Geol. 294, 106387 https://doi.org/10.1016/j.enggeo.2021.106387.

Cunningham, A.B., Phillips, A.J., Troyer, E., Lauchnor, E., Hiebert, R., Gerlach, R., Spangler, L., 2014. Wellbore leakage mitigation using engineered biomineralization. Energy Procedia 63, 4612–4619. https://doi.org/10.1016/j.egypro.2014.11.494.

DeJong, J.T., Mortensen, B.M., Martinez, B.C., Nelson, D.C., 2010. Bio-mediated soil improvement. Ecol. Eng. 36, 197–210. https://doi.org/10.1016/j.ecoleng.2008.12.029.

El Mountassir, G., Lunn, R.J., Moir, H., Maclachlan, E., 2014. Hydrodynamic coupling in microbially mediated fracture mineralization: Formation of self-organized groundwater flow channels. Water Resour. Res. 50, 1–16. https://doi.org/10.1002/2013WR013578.

Fan, T.X., Chow, S.K., Zhang, D., 2009. Biomorphic mineralization: from biology to materials. Prog. Mater. Sci. 54 (5), 542–659. https://doi.org/10.1016/j.pmatsci.2009.02.001.

Holt, R.M., Fjær, E., Stenebråten, J.F., Nes, O., 2015. Brittleness of shales : relevance to borehole collapse and hydraulic fracturing. J. Pet. Sci. Eng. 131, 200–209. https://doi.org/10.1016/j.petrol.2015.04.006.

Kirkland, C.M., Norton, D., Firth, O., Eldring, J., Cunningham, A.B., Gerlach, R., Phillips, A.J., 2019. Visualizing MICP with X-ray μ-CT to enhance cement defect sealing. Int. J. Greenh. Gas Control 86, 93–100. https://doi.org/10.1016/j.ijggc.2019.04.019.

Liu, K.S., Tian, D.L., Jiang, L., 2017. Frontier of Inorganic Synthesis and Preparative Chemistry (I) Biomimetic Synthesis. In: Modern Inorganic Synthetic Chemistry, Second edition. https://doi.org/10.1016/B978-0-444-63591-4.00024-0.

Liu, B., Zhu, C., Tang, C.S., Xie, Y.H., Yin, L.Y., Cheng, Q., Shi, B., 2020. Bio-remediation of desiccation cracking in clayey soils through microbially induced calcite precipitation (MICP). Eng. Geol. 264, 105389 https://doi.org/10.1016/j.enggeo.2019.105389.

Liu, B., Xie, Y.H., Tang, C.S., Pan, X.H., Jiang, N.J., Singh, D.N., Cheng, Y.J., Shi, B., 2021. Bio-mediated method for improving surface erosion resistance of clayey soils. Eng. Geol. 293, 106295 https://doi.org/10.1016/j.enggeo.2021.106295.

Matsubara, H., 2021. Stabilisation of weathered limestone surfaces using microbially enhanced calcium carbonate deposition. Eng. Geol. 284, 106044 https://doi.org/10.1016/j.enggeo.2021.106044.

Meng, F., Zhou, H., Zhang, C., 2015. Evaluation Methodology of Brittleness of Rock based on Post-Peak stress - Strain Curves. Rock Mech. Rock. Eng. 1787-1805 https://doi.org/10.1007/s00603-014-0694-6.

Meng, H., Shu, S., Gao, Y., Yan, B., He, J., 2021a. Multiple-phase enzyme-induced carbonate precipitation (EICP) method for soil improvement. Eng. Geol. 294, 106374 https://doi.org/10.1016/j.enggeo.2021.106374.

Meng, F., Wong, L.N.Y., Zhou, H., 2021b. Rock brittleness indices and their applications to different fields of rock engineering: a review. J. Rock Mech. Geotech. Eng. 13 (1), 221–247. https://doi.org/10.1016/j.jrmge.2020.06.008.

Minto, J.M., MacLachlan, E., El Mountassir, G., Lunn, R.J., 2016. Rock fracture grouting with microbially induced carbonate precipitation. Water Resour. Res. 52, 8827–8844. https://doi.org/10.1002/2016WR018884.

Minto, J.M., Hingerl, F.F., Benson, S.M., Lunn, R.J., 2017. X-ray CT and multiphase flow characterization of a 'bio-grouted' sandstone core: the effect of dissolution on seal longevity. Int. J. Greenh. Gas Control 64, 152–162. https://doi.org/10.1016/j.ijggc.2017.07.007.

Mortensen, B.M., Haber, M.J., Dejong, J.T., Caslake, L.F., Nelson, D.C., 2011. Effects of environmental factors on microbial induced calcium carbonate precipitation. J. Appl. Microbiol. 111, 338–349. https://doi.org/10.1111/j.1365-2672.2011.05065.x.

Phillips, A.J., Lauchnor, E., Eldring, J., Esposito, R., Mitchell, A.C., Gerlach, R., Cunningham, A.B., Spangler, L.H., 2013. Potential CO_2 leakage reduction through biofilm-induced calcium carbonate precipitation. Environ. Sci. Technol. 47 (1), 142–149. https://doi.org/10.1021/es301294q.

Phillips, A.J., Troyer, E., Hiebert, R., Kirkland, C., Gerlach, R., Cunningham, A.B., Spangler, L., Kirksey, J., Rowe, W., Esposito, R., 2018. Enhancing wellbore cement integrity with microbially induced calcite precipitation (MICP): a field scale demonstration. J. Pet. Sci. Eng. 171, 1141–1148. https://doi.org/10.1016/j.petrol.2018.08.012.

Rebata-Landa, V., 2007. Microbial Activity in Sediments: Effects on Soil Behavior. Dr. Diss. Georg. Inst. Technol, Atlanta, GA.

Salifu, E., MacLachlan, E., Iyer, K.R., Knapp, C.W., Tarantino, A., 2016. Application of microbially induced calcite precipitation in erosion mitigation and stabilisation of sandy soil foreshore slopes: a preliminary investigation. Eng. Geol. 201, 96–105. https://doi.org/10.1016/j.enggeo.2015.12.027.

Shaffer, G., 2010. Long-term effectiveness and consequences of carbon dioxide sequestration. Nat. Geosci. 3 (7), 464–467. https://doi.org/10.1038/ngeo896.

Sheng, G.P., Yu, H.Q., Li, X.Y., 2010. Extracellular polymeric substances (EPS) of microbial aggregates in biological wastewater treatment systems: a review. Biotechnol. Adv. 28, 882–894. https://doi.org/10.1016/j.biotechadv.2010.08.001.

Song, C., Elsworth, D., 2018. Strengthening mylonitized soft-coal reservoirs by microbial mineralization. Int. J. Coal Geol. 200, 166–172. https://doi.org/10.1016/j.coal.2018.11.006.

Song, C., Elsworth, D., 2020. Microbially Induced Calcium Carbonate plugging for Enhanced Oil Recovery. Geofluids. https://doi.org/10.1155/2020/5921789.

Song, C., Liu, S., 2020. A Novel Approach of Bulk Strength Enhancement through Microbially-Mediated Carbonate Cementation for Mylonitic Coal. Geomicrobiol J. 37 (8), 726–737. https://doi.org/10.1080/01490451.2020.1764675.

Song, C., Elsworth, D., Zhi, S., Wang, C., 2019. The influence of particle morphology on microbially induced $CaCO_3$ clogging in granular media. Mar. Georesources Geotechnol. 39 (1), 74–81. https://doi.org/10.1080/1064119X.2019.1677828.

Song, C., Zhi, S., Feng, G., Lin, J., 2021. Enhancing potential of hydrofracturing in mylonitic coal by biocementation. Energy Sci. Eng. 9 (4), 565–576. https://doi.org/10.1002/ese3.860.

Sutton, S., 2011. Measurement of microbial cells by optical density. J. Valid. Techn. 17 (1), 46–49. https://doi.org/10.1177/002215549904700703.

Tobler, D.J., Maclachlan, E., Phoenix, V.R., 2012. Microbially mediated plugging of porous media and the impact of differing injection strategies. Ecol. Eng. vol. 42, 270–278. https://doi.org/10.1016/j.ecoleng.2012.02.027.

Tobler, D.J., Cuthbert, M.O., Phoenix, V.R., 2014. Transport of Sporosarcina pasteurii in sandstone and its significance for subsurface engineering technologies. Appl. Geochem.. 42, 38–44. https://doi.org/10.1016/j.apgeochem.2014.01.004.

Tobler, D.J., Minto, J.M., El Mountassir, G., Lunn, R.J., Phoenix, V.R., 2018. Microscale Analysis of Fractured Rock Sealed with Microbially Induced $CaCO_3$ Precipitation: Influence on Hydraulic and Mechanical Performance. Water Resour. Res. 54, 8295–8308. https://doi.org/10.1029/2018WR023032.

Tourney, J., Ngwenya, B.T., 2009. Bacterial extracellular polymeric substances (EPS) mediate $CaCO_3$ morphology and polymorphism. Chem. Geol. 262, 138–146. https://doi.org/10.1016/j.chemgeo.2009.01.006.

Van Paassen, L., 2009. Biogrout: Ground Improvement by Microbially Induced Carbonate Precipitation. Delft University of Technology. https://doi.org/10.1111/idj.12061.

Wang, S., Elsworth, D., Liu, J., 2011. Permeability evolution in fractured coal: the roles of fracture geometry and water-content. Int. J. Coal Geol. 87 (1), 13–25. https://doi.org/10.1016/j.coal.2011.04.009.

Wu, J., Wang, X. Bin, Wang, H.F., Zeng, R.J., 2017. Microbially induced calcium carbonate precipitation driven by ureolysis to enhance oil recovery. RSC Adv. 7, 37382–37391. https://doi.org/10.1039/c7ra05748b.

Wu, C., Chu, J., Wu, S., Hong, Y., 2019. 3D characterization of microbially induced carbonate precipitation in rock fracture and the resulted permeability reduction. Eng. Geol. 249, 23–30. https://doi.org/10.1016/j.enggeo.2018.12.017.

Yasuhara, H., Kinoshita, N., Lee, D.S., Choi, J., Kishida, K., 2017. Evolution of mechanical and hydraulic properties in sandstone induced by simulated mineral trapping of CO_2 geo-sequestration. Int. J. Greenh. Gas Control 56, 155–164. https://doi.org/10.1016/j.ijggc.2016.11.018.

Zhi, S., Elsworth, D., Liu, L., 2019. W-shaped permeability evolution of coal with supercritical CO_2 phase transition. Int. J. Coal Geol. 211, 103221. https://doi.org/10.1016/j.coal.2019.103221.